Bulletin of Engineering Geology and the Environment
https://doi.org/10.1007/s10064-020-02039-8

ORIGINAL PAPER

Characterization of the interface between concrete pile and coral reef calcarenite using constant normal stiffness direct shear test

Haifeng Liu [1,2] · Changqi Zhu [1] · Ren Wang [1,2] · Xiang Cui [1,3] · Tianmin Wang [1,3]

Received: 3 April 2020 / Accepted: 30 October 2020

Abstract

This research aims to study the bearing capacity of pre-bored rock-socketed concrete pile on coral reef calcarenite. Constant normal stiffness direct shear test is performed on the interface between the pile and the coral reef calcarenite sample. Observations are made towards the friction mechanism of the pile-rock interface and the consequent shear dilation behaviors. It is shown that the shear failure occurs exclusively inside the coral reef calcarenite. This is attributed to the diffusion and agglomeration of cement paste in the highly porous coral reef calcarenite during the construction. The shear strength of the pile-rock interface increases as the applied normal stress increases. The dilation of the shear failure surface after the peak strength decreases as the applied normal stress increases. When the applied normal stress amounts to 4 MPa, shrinkage is observed for the shear failure surface. When the pile-rock interface slides, the residual shear strength of the interface increases as the applied normal stress increases. Meanwhile, the curve of the residual shear strength versus the shear displacement is affected by the shape and the roughness of the shear failure surface and it fluctuates under different levels of normal stress.

Keywords Coral reef calcarenite · Rock-socketed concrete pile · Constant normal stiffness direct shear test · Shear dilation

Introduction

Coral reef is formed after the corpse of the reef-building coral undergoes a long-lasting geological process. Coral reef is mainly distributed in the tropical marine regions between the north and south latitudes. The famous Great Barrier Reef of Australia and the Maldives Archipelago are both typical coral reef terrains (Wang et al. 1997; Zhao 1996).

As more and more engineering projects are introduced to the coral reef terrain around the world, pile foundation that is built on the cemented calcareous sediment of the coral reef (calcarenite) is gaining more and more attention from engineers and researchers. Successful applications of pile foundation on the coral reef terrain include the NRA platform of Australia's northwest continental shelf and the Sinamale Bridge of Maldives (Nyland 1988; Zhu et al. 2017). Researchers have carried out on-site drilling, geophysical survey, and laboratory-based physical and mechanical tests for the calcarenite, which is a kind of weakly cemented and highly compressible low strength bio sediment. It is found that the calcarenite consists of glued granules. The granules are the debris of the reef-building corals. The glue is the carbonate minerals, such as the aragonite and the high magnesium calcite. The granules have a wide range of radius and are moderately or poorly sorted. Nothing special can be observed in terms of the size distribution and the orientation of the granules (Zhu et al. 2016, 2017; Zhang 1985; Rubbert 1974; Given and Wilkinson 1985).

Lerouell and Vaughan (1990) and Lagioia and Nova (1995) investigated the bio calcarenite in Italy. It is revealed that the density and the degree of cementation are the main factors that control the mechanical properties of the calcarenite. However, because of the highly heterogeneous structure of the calcarenite, it is not an easy task to obtain representative samples and get consistent test results.

Zhu et al. (2016) performed laboratory tests to investigate the physical and mechanical properties of the calcareous

✉ Haifeng Liu
hfliu@whrsm.ac.cn

✉ Changqi Zhu
cqzhu@whrsm.ac.cn

[1] State Key Laboratory of Geomechanics and Geotechnical Engineering, Institute of Rock and Soil Mechanics, Chinese Academy of Sciences, Wuhan 430071, China

[2] Innovation Academy of South China Sea Ecology and Environmental Engineering, Chinese Academy of Sciences, Guangzhou 510301, China

[3] University of Chinese Academy of Sciences, Beijing 100049, China

Published online: 11 November 2020

calcarenite that were sampled from the Palm Island and the Rocky Island in the South China Sea. The tested samples demonstrate intergranular contact cementation and high porosity. The sample from the Rocky Island has a porosity of 53.8% while the sample from the Palm Island has a porosity of 18.4%. The uniaxial compression of the saturated samples in a servo loading system indicates that the behaviors of the samples are similar to that of granular material. That is to say, during the compression, the densification starts from the far ends of the samples. The stress-strain curve demonstrates two peaks and high residual strength. The Brazilian test of the samples shows that the fracture tends to propagate along the cementation between the granules. Therefore, Zhu proposes to quantify the strength of the cementation using the tensile strength.

The bearing capacity of the pile foundation in the calcarenite is also investigated. While constructing the pile foundation of the North Rankin A oil drilling platform of Australia in 1988, William and Van der Zwaag (1988) carried out the static load tests on steel pipe piles. The steel pipe piles have a length of 2.3 m and a radius of 450 mm. They are socketed into the moderately cemented calcarenite whose depth extends up to 118.9–147.4 m bellow the mudline. As the test indicates, the skin friction of the steel pipe piles ranges between 438 and 685 kPa. The skin friction reaches its peak value when the pile settlement amounts to 2.3–5 mm. The residual skin friction after the peak is 31–48% of the peak value.

In terms of the model test of the pile foundation, researchers carried out the push-in test of pile in the artificially cemented calcarenite. The result shows that the growth of the skin friction of the pile is sublinear to the increase of the pile settlement (Zhao and Airey 1992; Huang and Airey 1993; Lagioia et al. 1998; Yeoh and Airey 1998; Carter et al. 1999; Cuccovillo and Coop 1999).

Gunasena et al. (1995) carried out the post-grouting for the pile foundation in the artificial calcarenite. They intend to find out how the post-grouting can enhance the skin friction of the pile. Their research shows that the degree of cementation and the compressibility of the coral reef calcarenite are the dominant factors for the bearing capacity of the piles that undergo post-grouting.

Thus, it can be seen, coral reefs have thick covering layer of cemented calcareous sediment (calcarenite), which can be used as the foundation bearing layer of superstructure. The strength characteristic and friction performance of pile-rock interface all affect the safety and stability of construction. Therefore, it is of great theoretical significance and engineering application value to carry out relevant experimental research on the pile foundation in this stratum.

It is worth noting that the interface between concrete and surrounding rock (calcarenite) is considered to be rough. When the socketed pile is loaded vertically, the side shear resistance develops as a function of the variable normal stress associated with the dilation of the rough joint surface. And the development of shear resistance is a function of constant normal stiffness (CNS) (Indraratna et al. 1998).

In the presented work, the calcarenite sampled from Yongxing Island in the South China Sea undergoes the constant normal stiffness direct shear test. Through this, the friction mechanism between the calcarenite and the concrete pile can be revealed. Furthermore, the impact of the normal stress on the shear dilation of the pile-rock interface and the residual skin friction of the pile can be investigated.

Physical and mechanical properties of the samples

The calcarenite samples are drilled from the shallow strata of Yongxing Island, which are essentially cemented calcareous sand. Carbide drill and wireline coring tool are used in the field drilling, and the diameter of the core is 70 mm. Due to low strength, the cores are relatively broken, and the length of each section of core is generally between 60~150 mm. Calcarenite cores are placed in the core box to reduce the disturbance and damage during transportation.

In order to apply the laboratory tests, the calcarenite core samples from Yongxing Island are cut into standard cylinder samples. Standard cylinder specimen of calcarenite is obtained by drilling along the longitudinal direction of the core, and then cutting at the ends. The cylinder samples have a diameter of 50 mm and a height of 100 mm (see Fig. 1). The physical and mechanical properties to be tested include the dry density, the saturated water absorption, the porosity, and the saturated uniaxial compression strength.

Specific gravity (GS)

The measurement of the special gravity of the calcarenite is performed in accordance with the Specification of Soil Test of China (SL237-1999). The calcarenite sample is ground into powders no larger than 0.075 mm in diameter beforehand. The pycnometer test using kerosene quantifies the averaged special gravity of the calcarenite to be 2.65.

Fig. 1 Calcarenite sample

Density and porosity

The measurement of the density is performed in accordance with the Code for Rock Tests of Hydroelectric and Water Conservancy Engineering of China (DL/T5368-2007). Firstly, the precise dimensions of the standard cylinder sample are determined using a vernier caliper that provides a precision to 0.02 mm. The volume of the sample can thus be calculated. Afterwards, the sample is dried with a temperature of 105 °C until the weight does not vary. The dried sample is weighed using a balance with a minimum increment of 0.01 g. Finally, the dry density of the sample is the quotient of dividing the weight by the volume.

After measuring the dry density, the sample is exposed to the moisture. Once the weight of the sample no longer varies after absorbing the moisture, the sample is placed inside a vacuum saturation tank. The tank is evacuated to − 100 kPa for 4 h. Afterwards, the pressure of the vacuum saturation tank is resumed to normal and the sample is maintained therein for another 4 h. At the end, the sample is taken out of the tanker, cleared of the excess surface water, and weighted using a balance with a minimum increment of 0.01 g. The saturated water absorption and the saturated density can be calculated thereof. The test results are listed in Table 1.

Saturated uniaxial compression strength

The uniaxial compression test of the sample under water saturated condition is performed using the RMT-150C testing machine. It is a digital electro-hydraulic servo loading system developed by the State Key Laboratory of Geomechanics and Geotechnical Engineering of China. The sample to be tested needs to be morphed into a cylinder with a diameter of 50 mm and a height of 100 mm. The displacement control is adopted with a loading rate of 0.002 mm/s. The obtained stress-strain curves are plotted in Fig. 2. As can be inferred from Fig. 2, the saturated uniaxial compression strength (UCS) of the calcarenite sample is 1.0 MPa, the Young's modulus is 1.1 GPa, and the Poisson's ratio ν is 0.03.

The obtained stress-strain curves are similar to those reported by Zhu et al. (2016) when they performed the saturated uniaxial compression test on the calcirudite sample from Rocky Island in the South China Sea. For the calcarenite and the calcirudite, which are highly porous and poorly cemented, strain hardening after the first peak stress can be frequently observed.

Shear test

Preparation of the shear sample

The steps of preparing the shear sample are as follows:

I. A cylindrical segment with a height of 60~ 70 mm is cut off from the calcarenite core sample which diameter is 70 mm. The obtained cylinder sample is then bisected into two half cylinder samples along the longitudinal direction.

II. One of the two half cylinder samples is chosen for test and it is placed inside a cubic mold box that is made of cast iron and has a cross section of 150 mm × 150 mm. The half cylinder sample is situated at the center of the mold box with the cutting profile facing upward. Cement paste is then poured into the mold box until the level of the cement paste is 5 mm below the cutting profile of the half cylinder sample. The obtained shear sample is then cured so that the cement paste can have adequate strength.

III. A specially designed gasket (shown in Fig. 3) is applied before grade C30 concrete is poured into the mold box to form the other half of the shear sample. As can be seen from Fig. 3, the gasket results in a neck with a thickness of 10 mm between the upper and lower pedestals. The lower half of the neck is the calcarenite and the upper half of the neck is the concrete.

In this way, the shear plane of the shear specimen is the bond surface between the cut surface along the longitudinal direction of the half cylinder and the concrete.

IV. After the concrete gains adequate strength, the mold box and the gasket are removed. The obtained shear sample is then placed in a curing box for 28 days. Figure 4 shows the completed shear sample.

This kind of preparation method can make full use of the limited sample condition to carry out the research, and obtain the rule of pile-rock interface friction. It is also adopted by Zhu (2006) and Johnston (1988).

Equipment and test condition

The constant normal stiffness direct shear test is performed using the RJST-616 shear test machine. It is developed by the State Key Laboratory of Geomechanics and Geotechnical Engineering of China. A sketch of how the shear test machine works is shown in Fig. 5. Using a servo controller, the shear test machine can apply constant normal load (CNL) and constant normal stiffness (CNS, in the range of 10~5000 kN/mm, equivalent to installing spring constraints in the normal direction). Either the force or the

Table 1 Physical properties of the calcarenite sample

Rock type	Dry density (g/cm^3)	Saturated density (g/cm^3)	Porosity (%)	Saturated water absorption (%)
Calcarenite	1.65	1.96	37.7	18.8

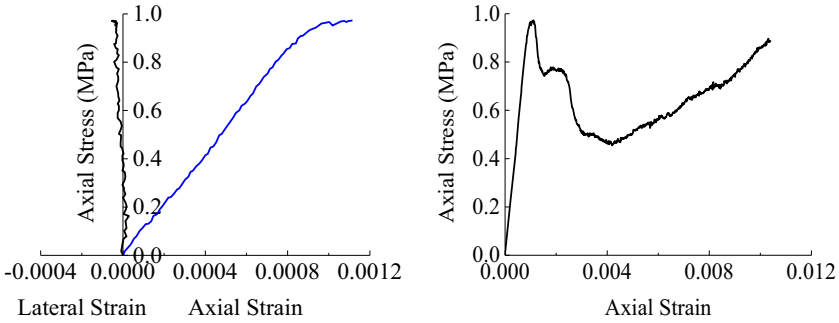

(a) Stress-strain curve before peak strength (b) Complete stress-strain curve

Fig. 2 Stress-strain curve of the calcarenite sample under uniaxial compression. **a** Stress-strain curve before peak strength. **b** Complete stress-strain curve

displacement control can be applied in both the normal and the shear constraints. The maximum force that can be exerted is 200 kN for the normal constraint and 300 kN for the shear constraint. The machine will record the force and the displacement in both the normal and the shear constraints with a frequency of 10 Hz (Cui et al. 2018).

The normal stiffness K to be exerted in the shear test is calculated according to the solution of the thick-walled cylinder in the theory of elasticity (citation):

$$K = \frac{\Delta\sigma_n}{\Delta r} = \frac{1}{r} \cdot \frac{E_m}{(1+\nu_m)} \tag{1}$$

where E_m is the Young's modulus of the rock, ν_m is the Poisson's ratio of the rock, r is the diameter of the pile, Δr is the increment of the diameter of the pile, and $\Delta\sigma_n$ is the increment of the normal stress. In the presented work, the diameter of the pile is chosen to be 600 mm, and the Young's modulus and the Poisson's ratio of the calcarenite that holds the pile are determined in the "Saturated uniaxial compression strength" section. According to Eq. (1), the normal stiffness to be imposed in the direct shear test is 1.78 MPa/mm. For convenience, it is rounded to be 2.0 MPa/mm.

The normal stiffness to be set for the RJST-616 shear test machine is K' and it needs to be calibrated from K by multiplying with the shear area S of the sample, i.e.,

$$K' = K \cdot S \tag{2}$$

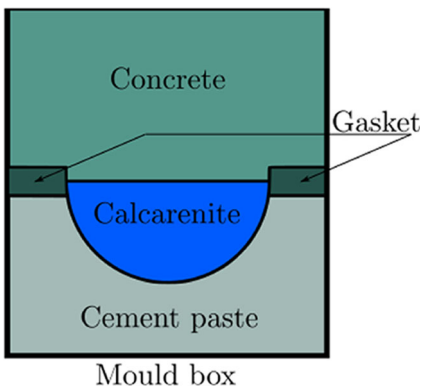

Fig. 3 Sketch for the preparation of the shear sample

Now that the normal stiffness remains constant throughout the shear test, three different levels of initial normal stress (i.e., 1 MPa, 2 MPa, and 3 MPa) are considered to understand how the peak shear strength of the pile-rock interface evolves under different levels of normal stress. After taking into consideration the effect of the loading rate on the result of the shear test (Tang and Wong 2016), the target normal stress (to be multiplied with the shear area) is exerted with a loading rate of 0.1 kN/s before the shear deformation is introduced with a rate of 0.001 mm/s.

Experiment results

Shear stress in the CNS shear test

Figure 6a plots the curves of the shear stress versus the shear displacement for the pile-rock interface under the condition of

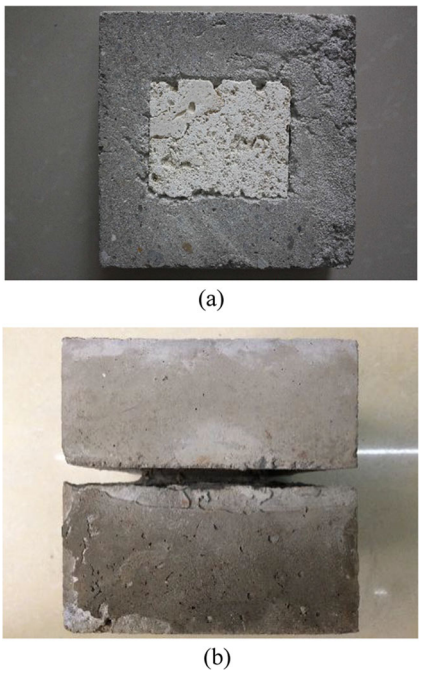

(a) (b)

Fig. 4 The shear sample. **a** The lower half of the shear sample with the calcarenite embedded inside the cement paste. **b** The completed shear sample

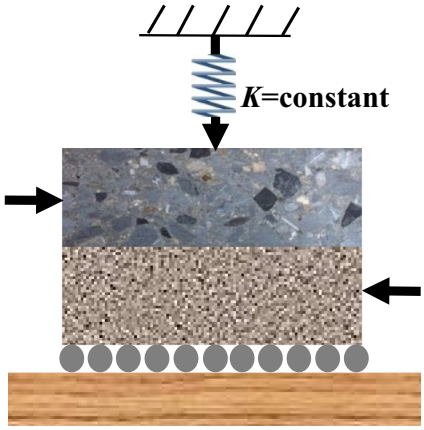

Fig. 5 Schematic diagram of shear test machine

constant normal stiffness. As can be seen, although the imposed normal stresses are quite different, the curves maintain similar shapes. Four phases can be identified for each curve, i.e., the adjustment phase, the climbing phase, the declining phase, and the sliding phase.

In the adjustment phase, the artifact of the pile-rock interface is eliminated. During this phase, the shear stress increases slowly due to the low shear stiffness of the pile-rock interface.

In the climbing phase, steep growth is observed for the curve. The pile-rock interface sustains failure when the level of the shear stress reaches the shear strength of the interface. The shear displacement upon the onset of shear failure for all the scenarios is less than 1.2 mm. Moreover, the larger the normal stress is, the larger the peak shear stress is.

In the declining phase, the shear stress decreases. As can be seen, the larger the normal stress is, the more slowly the shear stress decreases.

In the sliding phase, the pile-rock interface slides after the shear failure. As can be seen, the larger the normal stress is, the larger the residual shear strength is. Moreover, the shear dilation resulted from the shear failure depends on the shape of the failure surface. For all the scenarios, the residual shear strength is almost constant.

Shear stress decrease rate in the post-peak phase

The curves of the shear stress versus the shear displacement in Fig. 6a can be approximated using the idealized curve in Fig. 7.

The declining rate of the shear stress after the peak can be measured from the segment A–B in Fig. 7 by defining the declining rate R:

$$R = \frac{\log\left|\frac{\tau_p - \tau_r}{(S_p - S_r)/L}\right|}{10} \tag{3}$$

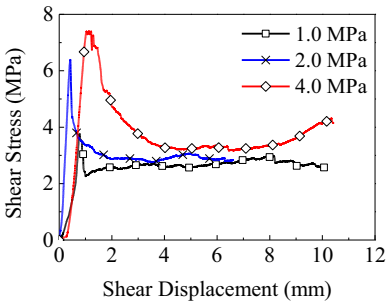

(a) Shear stress versus shear displacement

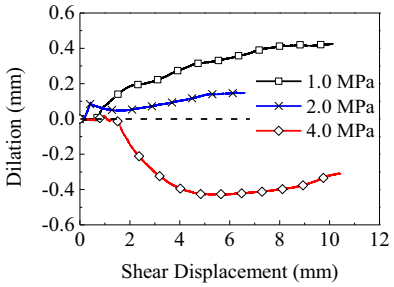

(b) Dilation versus shear displacement

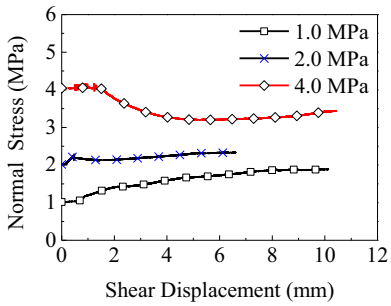

(c) Normal stress versus shear displacement

Fig. 6 Results of the constant normal stiffness direct test. **a** Shear stress versus shear displacement. **b** Dilation versus shear displacement. **c** Normal stress versus shear displacement

where τ_p (MPa) and τ_r (MPa) represent the peak shear strength and the initial residual shear strength; S_p (mm) and S_r (mm) are the corresponding shear displacements; L (mm) is the length of the shear plane. Table 2 lists the declining rate of the shear stress for all the loading scenarios. As is shown in Fig. 8, the

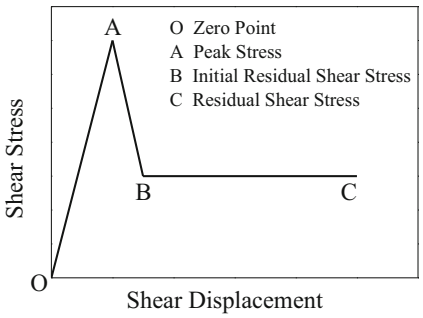

Fig. 7 Idealized approximation of the shear stress-shear displacement curve

Table 2 Calculation of shear stress declining rate

Initial normal stress (MPa)	1.0	2.0	4.0
Length of shear plane L (mm)	70	70	60
Peak shear strength τ_p (MPa)	3.78	6.39	7.40
Initial residual shear strength τ_r (MPa)	2.26	2.87	3.25
Shear displacement of peak shear strength S_p (mm)	0.78	0.42	1.13
Shear displacement of initial residual shear strength S_r (mm)	1.01	2.00	4.06
Declining rate of the shear stress R	0.27	0.22	0.19

declining rate of the shear stress can be related to the initial normal stress using a power function.

Dilation and normal stress in the CNS shear test

Figure 9 depicts the curves of the shear dilation versus the shear displacement for all the loading scenarios before the peak shear strength is reached. Shear shrinkage that is less than 0.01 mm can be observed in the adjustment phase. Afterwards, shear dilation occurs in all the loading scenarios. The shear dilation after the peak shear strength can be seen from Fig. 6b. As is shown there, in case the applied initial normal stress is 1.0 MPa and 2.0 MPa, the pile-rock interface sustains shear dilation throughout the shear failure. Moreover, the larger the normal stress is, the smaller the shear dilation is. In case the applied initial normal stress is 4.0 MPa, the pile-rock interface switches from shear dilation to shear shrinkage. During the sliding phase, the shear dilation of the pile-rock interface in all the loading scenarios slightly increases.

In the meanwhile, because applying constant normal stiffness is equivalent to installing spring constraints in the normal direction, the normal stress also needs be monitored throughout the shear test. Figure 6c demonstrates the evolvement of the normal stress during the shear test. The evolvement of the normal stress (see Fig. 6c) is similar to that of the dilation (see Fig. 6b). More specifically, the normal stress increases in case of shear dilation (e.g., the loading scenarios with an initial normal stress of 1.0 MPa and 2.0 MPa) and decreases in case of shear shrinkage (e.g., the loading scenario with an initial normal stress of 4.0 MPa).

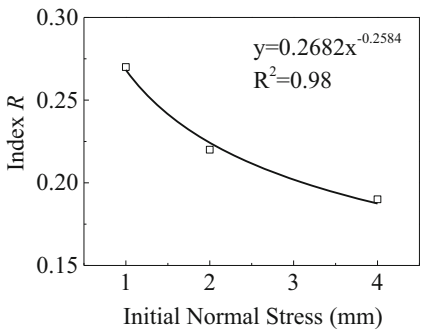

Fig. 8 Relationship between the declining rate R and the initial normal stress

As shown in Fig. 10, the relationship between normal stress and dilation of the three cases for various initial normal stresses are demonstrated directly. In the CNS controlling shear test, the normal stress and the normal displacement are well proportioned in the process according to the input value of normal stiffness K. And the slopes of the fitting straight line of the test curve are both 2.0 MPa/mm.

Shear behavior of test sample under CNS condition

The normal stress versus shear stress path under CNS condition is shown in Fig. 11. In each case, the shear stress initially rises before the peak shear strength. For different case of initial normal stress, the trend of normal stress after peak shear strength is different. In case the applied initial normal stress is 4.0 MPa, normal stress decreases in the post-peak stage while this index increases in the case of 1.0 MPa and 2.0 MPa.

This article refers to the research ideas of Indraratna (1998). Through the linear fitting of the peak shear strength point, the linear envelope of the shear stress peak strength in the shear process is obtained (see Fig. 11).The internal friction angle of pile-rock interface is 49.72° and the cohesion is 2.99 MPa.

Pile-rock interface during the pre-peak and post-peak phases

The scanning electron microscope (SEM) is applied to investigate the pile-rock interface. The high porosity of the calcarenite allows for significant diffusion of the cement paste, which results in the formation of stronger cementation between the pile and the calcarenite. This is revealed in the

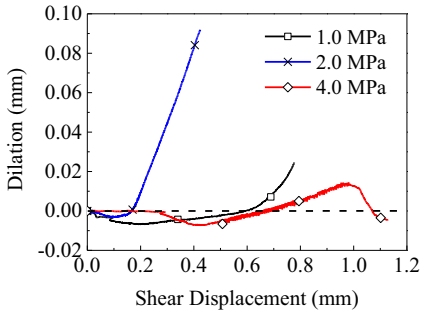

Fig. 9 Dilation before the peak shear strength

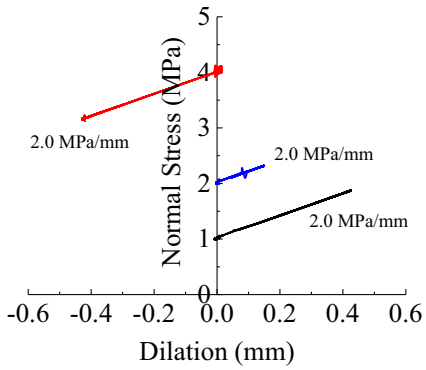

Fig. 10 Relationships between normal stress and dilation

SEM image of Fig. 12, which shows the cement paste filling the pores of the calcarenite. Meanwhile, due to the capillary effect of the porosity of the calcarenite, the cement paste at the proximity of the pile-rock interface has a smaller water-cement ratio, which leads to higher shear strength after curing. Consequently, the shear failure tends to occur within the calcarenite, which is of lower strength.

Figure 13 shows the failure surfaces after the shear tests. The failure surfaces are a mixture of the calcarenite and the concrete. Due to the roughness of the failure surfaces, the residual shear strength fluctuates during the sliding phase (see Fig. 6a). For the shear test with an initial normal stress of 4.0 MPa, the failure surface is of dome shape and the residual shear strength slightly increases with the increasing shear displacement.

Residual shear strength

As can be inferred, the residual shear strength of the pile-rock interface is influenced by both the level of the initial normal stress and the roughness of the shear failure surface. Moreover, the roughness of the shear failure surface leads to the fluctuation of the residual shear strength as the shear displacement increases.

The bearing capacity for the concrete pile in coral reef calcarenite can be determined by referring to the initial residual shear strength τ_r (i.e., point B in Fig. 7).

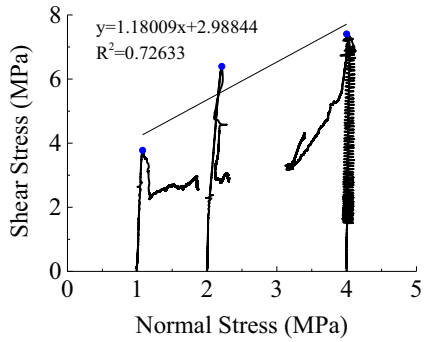

Fig. 11 Shear stress versus normal stress path under CNS condition

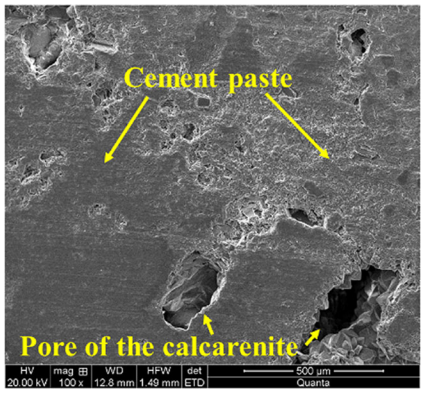

Fig. 12 Microstructure of the interface between the calcarenite and the concrete

Figure 14 shows that the initial residual shear strength τ_r can be related to the initial normal stress using a logarithmic function.

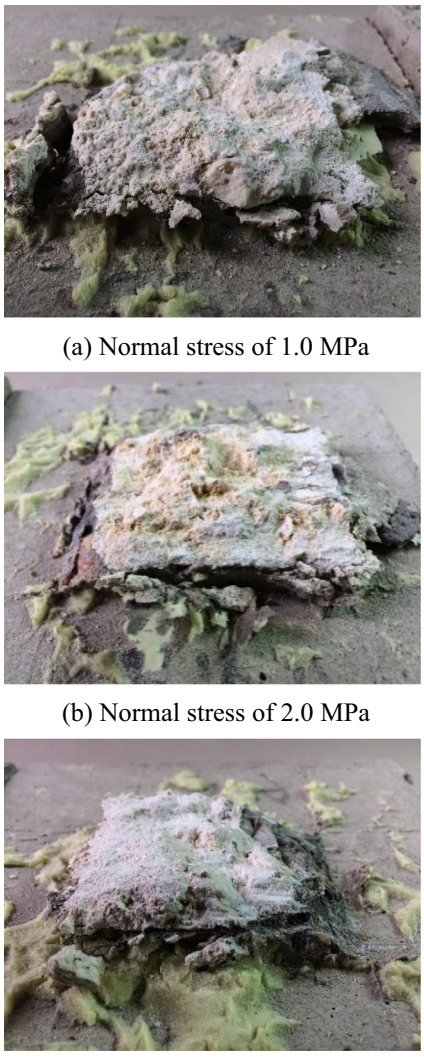

(a) Normal stress of 1.0 MPa

(b) Normal stress of 2.0 MPa

(c) Normal stress of 4.0 MPa

Fig. 13 Shear failure surface of the shear test under different initial normal stress. **a** Normal stress of 1.0 MPa. **b** Normal stress of 2.0 MPa. **c** Normal stress of 4.0 MPa

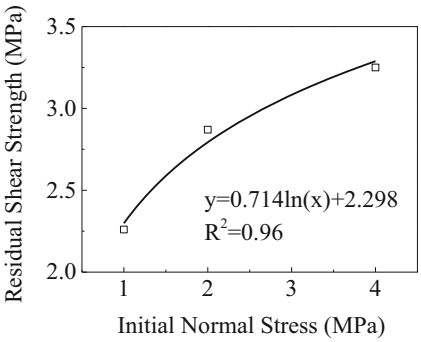

Fig. 14 Relationship between the initial residual shear strength and the initial normal stress

Due to the scale effect and test condition, the peak shear strength and residual shear strength of this test are larger than those of Williams and Van der Zwaag (1988). In this test, the shear displacement of the specimens at peak shear strength are less than 1.2 mm, while in the field tests of Williams and Van der Zwaag (1988), the displacement are 2.3~5 mm. However, the development trend of friction of pile-rock interface is the same. The residual shear strengths are both 30–60% of the peak shear strength.

It is worth noting that the performed shear test of the pile-rock interface is relatively small in scale. In practical engineering, the interface between pile and rock is curved surface, and the developed area of pile-rock is larger than that of shear specimen. Therefore, the design value should base on the test results, taking into account the influence of size effect and multiplying by the corresponding size effect coefficient. When the residual shear strength obtained from the experiment is referred to in the practices of engineering scales, a scale down is necessary. And the size effect coefficient should be determined by comparing the shear test results with the field test results under the same formation condition.

Conclusions

The constant normal stiffness direct shear test is performed for the pile (concrete)-rock (calcarenite) interface. It is shown that the shear strength of the pile-rock interface is enhanced due to the diffusion of the cement paste in the porosity of the calcarenite. As a consequence, the shear failure tends to happen inside the calcarenite.

Under different initial normal stresses, the response curves of the shear stress versus the shear displacement maintain similar shapes. Four phases can be identified for each curve, i.e., the adjustment phase, the climbing phase, the declining phase, and the sliding phase. The declining rate of the shear stress after the peak is dependent on the initial normal stress. The larger the initial normal stress is, the more slowly the shear stress declines.

In the adjustment phase, minor shear shrinkage can be observed for the pile-rock interface. As the shear stress increases, the interface switches to shear dilation. The evolvement of the shear dilation of the pile-rock interface after the peak is dependent on the level of the normal stress. Specifically, as the initial normal stress increases, the shear dilation decreases and even switches to shear shrinkage.

In the sliding phase, the residual shear strength of the failure surface is influenced by both the roughness of the failure surface and the level of the normal stress. A fluctuation can be observed for the residual shear strength. Also, higher initial normal stress leads to higher residual shear strength.

It should be noted that coral reef calcarenite has strong structural characteristic, the strength of calcarenite of different structural types is different, and so as the shear characteristics of pile-rock interface. Liu (2020) has revealed the significant differences in shear strength between calcarenite and concrete of different structural types. Therefore, the test results cannot be simply extended to all kinds of calcarenite. Laboratory test, field test, and theoretical analysis should be carried out base on the specific formation condition.

Funding This study was financially supported by the Strategic Priority Research Program of the Chinese Academy of Sciences (Grant No. XDA13010201, XDA13010301), Self-Deployment Project of Innovation Academy of South China Sea Ecology and Environmental Engineering of the Chinese Academy of Sciences (Grant No. ISEE2020YB09), and the National Natural Science Foundation of China (Grant No. 41877271).

References

Carter JP, Airey DW, Fahey M (1999) A review of laboratory testing of calcareous soils. Proceedings of the second international conference on engineering for calcareous sediments. Bahrain 2:401–432

Cuccovillo T, Coop M (1999) On the mechanics of structured sands. Geotechnique 49(6):741–760

Cui GJ, Zhang CQ, Liu LP (2018) Study of effect of shear velocity on mechanical characteristics of bolt-grout interface. Rock Soil Mech 39(S1):275–281

DL/T5368-2007 Code for rock tests of hydroelectric and water conservancy engineering (2007). China Electric Power Press, Beijing

Given RK, Wilkinson BH (1985) Kinetic control of morphology, composition and mineralogy of abiotic sedimentary carbonates. J Sediment Petrol 55(1):109–119

Gunasena U, Joer HA, Randolph MF (1995) Design approach for grouted driven piles in calcareous soil. Proceedings of 27th Annual Offshore Technology Conference, Houston, pp 271–280

Huang JT, Airey DW (1993) Effects of cement and density on artificially cemented sand. Geotechn Eng Hard Soils-Soft Rocks 1:553–560

Indraratna B, Haque A, Aziz N (1998) Laboratory modelling of shear behaviour of soft joints under constant normal stiffness conditions. Geotech Geol Eng 16:17–44

Johnston IW, Novello EA, Carter JP et al (1988) Constant normal stiffness direct shear testing of calcarenite. Proceedings of the International Conference on Calcareous Sediments, Perth, Institution of Engineers, 2: pp 541–553

Lagioia R, Nova R (1995) An experimental and theoretical study of the behaviour of a calcarenite in triaxial compression. Geotechnique 45(4):633–648

Lagioia R, Borland JB, Delage P (1998) Pre-yield behaviour of Gravina calcarenite at small strains. The Geotechnics of Hard Soils-Soft Rocks, Proceedings of the 2nd International Symposium on Hard Soils-Soft Rocks, Naples, Italy, 1: pp 629–636

Leroueil S, Vaughan PR (1990) The general and congruent effort of structure in nature soils and weak rocks. Geotechnique 40(3):467–488

Liu HF, Zhu CQ, Wang R et al (2020) Shear test on reef limestone-concrete bonding interface. Rock Soil Mech 41(5):1540–1548

Nyland GW (1988) Detailed engineering geological investigation of North Rankin 'A' platform site. Proceedings of the International Conference on Calcareous Sediments, Perth, Institution of Engineers, 2: pp 503–512

Rubbert LF (1974) The natural history of crystalline calcium carbonate: effect of magnesium content and salinity. J Sediment Petrol 44(1): 40–53

SL237-1999 Specification of soil test (1999). China Water Power Press, Beijing

Tang ZC, Wong LNY (2016) Influences of normal loading rate and shear velocity on the shear behavior of artificial rock joints. Rock Mech Rock Eng 49(6):2165–2172 (in Chinese)

Wang R, Song CJ, Zhao HT, Zhu CQ et al (1997) The coral reef engineering geology of the Nansha Islands. Science Press, Beijing

Williams AF, Van der Zwaag GL (1988) Analysis and evaluation of grouted section tests. Proceedings of the International Conference on Calcareous Sediments, Perth, Institution of Engineers, 2: pp 493–502

Yeoh CK, Airey DW (1998) Drained cyclic response of an artificially cemented calcareous sand. The Geotechnics of Hard Soils-Soft Rocks, Balkema, 2: pp. 935–942

Zhang MS (1985) On problems of beachrock. Marine Geol Quat Geol 5(2):105–112 (in Chinese)

Zhao HT (1996) The natural geography of the Nansha Islands. Science Press, Beijing

Zhao MM, Airey DW (1992) Fatigue testing of an artificially cemented calcareous sand. Proceedings of the 2nd International Offshore and Polar Engineering Conference, San Francisco, 1: pp 424–429

Zhu ZD, Xing FD, Qu WP, Chen WZ (2006) Fractal description of shear strength of cementation plane between rock and concrete. Chin J Rock Mech Eng 25(S1):2910–2917

Zhu CQ, Liu HF, Zhou B (2016) Micro-structures and the basic engineering properties of beach calcarenites in South China Sea. Ocean Eng 3(114):224–235

Zhu CQ, Liu HF, Wang X, Meng QS, Wang R (2017) Engineering geotechnical investigation for coral reef site of the cross-sea bridge between Malé and Airport Island. Ocean Eng 12(146):298–310